Tightly-Coupled GPS/UWB-Ranging for Relative Navigation During Formation Flight

Jason N. Gross, Yu Gu, *West Virginia University*
Brandon Dewberry, *Time Domain*

BIOGRAPHY

Dr. Jason Gross is an assistant professor at West Virginia University (WVU) interested in research focused on improving PNT accuracy and robustness in GPS challenged environments. He received his Ph.D. in Aerospace Engineering from WVU in 2011, where he conducted research on sensor fusion navigation algorithms and flexible UAV avionics systems for fault-tolerant flight controls research. From 2011 to December 2013, he was a Research Technologist in the Near Earth Tracking Applications Group at Caltech's Jet Propulsion Laboratory (JPL), where he worked in the area of GNSS data analysis and processing algorithm development (i.e. GIPSY, Modernized GIPSY).

Dr. Yu Gu is an assistant professor at WVU interested in the areas of sensing and control, with applications to robotic systems. Gu earned a B.S degree in Automatic Controls from Shanghai University in 1996, a M.S. degree in Control Engineering from Shanghai Jiaotong University in 1999, and a Ph.D. degree in Aerospace Engineering from West Virginia University in 2004. He has managed many funded projects as the Principal Investigator (PI) or as a Co-PI, and has designed and managed over 450 outdoor flight tests and numerous indoor robot experiments, and led a robot development for the 2014 NASA Sample Return Robot Challenge to a successful Level 1 award.

Mr. Brandon Dewberry is the Chief Technology Officer (CTO) of Time Domain, a leader in pulsed Ultra Wideband (UWB) radio and radar technologies. As CTO Mr. Dewberry enjoys using his deep technical knowledge of UWB to solve new interesting problems while directing the companies' product and technology path. Prior to transitioning to Time Domain in 2000 Mr. Dewberry was a 'go-to' logic designer in the Instrumentation and Controls Division of NASA's Marshall Space Flight Center where he developed firmware for a number of Space Sciences instruments including the Differential Ion Flux Probe (DIFP) which flew on TSS-1 and the Suppression of Transient Accelerations by Levitation (STABLE) experiment which flew on STS-73/USML-02.

ABSTRACT

This paper considers tightly-coupled fusion of differential GPS (DGPS) and Impulse Radio Ultra-Wideband (IR-UWB) peer-to-peer ranging for the application of relative navigation of aircraft in close formation-flight. A simulation environment is developed and used to evaluate dynamic baseline estimation performance under various conditions including: varying multipath intensity, occurence of phase breaks, IR-UWB measurement noise and time-lag with respect to GPS. The incorporation of IR-UWB ranging is shown to offer improved 3-D relative positioning accuracy and robustness when faced with these common errors. Two formulations are presented and compared with and without the IR-UWB ranging source, including fixing integer phase biases with the Least-squares AMBiguity Decorrelation Adjustment (LAMBDA) method, and a differential method that does not require bias fixing and instead time differences two single-difference observations to eliminate phase ambiguities. In addition, trade-offs of integrating the IR-UWB with respect to measurement rate, communication throughput, and maximum distance are also presented. Potential applications of this technology are those that require accurate and robust relative navigation, including: cooperative remote sensing, distributed synthetic aperture radar, aircraft formation flight for fuel saving, collision avoidance, and aircraft traffic management, as well as extensions to ground (e.g. driverless cars) applications.

1 INTRODUCTION

1.1 Background and Motivation

The immediate motivation for this work is to provide a robust and accurate real-time relative navigation algorithm to support an ongoing research project at West Virginia University (WVU) in which wind gusts are cooperatively estimated and suppressed by a pair of close-formation flying small UAVs. The fast-dynamics and associated abrupt attitude changes of small UAV platforms often lead to GPS carrier phase loss-of-lock or cycle slips, and are therefore not, by themselves, ideal platforms for realizing the cm-level potential of differential carrier phase GPS relative navigation solutions. Because of this, UWB peer-to-peer ranging between UAVs is investigated in simulation to provide

an initial assessment of its expected benefit in the face of conditions that are challenging for traditional Differential GPS (DGPS) .

1.2 Previous Works

Recent studies have demonstrated the great potential of tightly-coupling UWB with GPS. For example, MacGougan et al. (MacGougan et al., 2010) used a network of UWB radios placed at surveyed and fixed locations to augment GPS, and demonstrated the effectiveness of tightly-coupling GPS and UWB range measurements to yield better accuracy and an improved ability to fix GPS integer phase biases during both static and kinematic applications. Improvements were especially significant during periods of poor satellite geometry. In their work, the accuracy improvement of the 'float' phase bias solution was noticeable when UWB measurements were included, and the LAMBDA method (Teunissen, 1995) was then employed to fix biases. Broshears' (Broshears, 2013) conducted an investigation of the potential for using UWB ranges between two GPS receivers to constrain the baseline and assist in reducing the ambiguity resolution search space with the constrained LAMBDA method. The approach showed promise over short baselines, and determined that the bias-fixing algorithm could tolerate up to 4-cm of UWB range error. Jiang (Jiang, 2012) demonstrated multiple benefits of tightly-coupled GPS/UWB when employing UWB at a traffic intersection in the context of supporting Vehicle-to-Infrastructure (V2I) relative positioning for an Intelligent Transport System (ITS). The work presented in this paper leverages these recent findings, but deviates from prior work by focusing on the specific problems associated with mobile Vehicle-To-Vehicle (V2V) relative navigation without the use of a fixed reference station.

DGPS tightly-coupled with Inertial Navigation Systems (INS) have demonstrated cm-level relative positioning between formation flying aircraft using commercial components. In particular, a system was developed for NASA Dryden's F-18 autonomous formation flight program and demonstrated 7-cm mean error with 13-cm standard deviation when compared to post-processed DGPS solutions that rely on a static reference station (Williamson et al., 1999) (Williamson et al., 2007). In this study, we choose to focus on the assessment of the potential improvements to relative positioning by introducing IR-UWB peer-to-peer range measurements tightly-coupled with DGPS between the aircraft, and leave the integration for INS as the next step.

The rest of this paper is organized as follows. Section 2 details the two different tightly-coupled DGPS/UWB sensor fusion approaches considered. Section 3 describes the WVU UAV research platform and Section 4 details the simulation environment developed for this study. Sections 5 discusses some practical tradeoffs on integrating the IR-UWB peer-to-peer ranging source. Section 6 presents the results of the simulation study and Section 7 discusses the study conclusions and future plans for working on this problem.

2 ALGORITHM FORMULATIONS

2.1 Tightly-Coupled Double-Difference GPS and Ultra-Wideband Ranging

The first formulation considered in this study includes the IR-UWB peer-to-peer range measurement as a direct measurement of the baseline distance between two GPS receivers in order to augment a local DGPS algorithm that estimates the the dynamic 3D relative position vector. The DGPS algorithm uses double-differenced GPS observables and fixes phase biases to integers using the Least-squares AMBiguity Decorrelation Adjustment (LAMBDA) method (Teunissen, 1995).

The observation model of the undifferenced GPS carrier-phase measurements are written as (Misra and Enge, 2006):

$$\phi = \lambda^{-1}[r + I_\phi + T_\phi] + \frac{c}{\lambda}(\delta t_u - \delta t^s) + N + \varepsilon_\phi \qquad (1)$$

where the carrier-phase, ϕ, is in units of cycles of the wavelength, λ, which is in units of meters. I refers to ionospheric delay in meters, T is the tropospheric delay in meters, c is the speed of light in m/s, δt are clock biases of the user's receiver u and satellite transmitter S in seconds, and ε represents the multipath error with units of meters. Additionally, the unknown number of integer cycles, N , which remains fixed as long a given link is continuously tracked is included in units of cycles.

The standard observables for local-area DGPS applications are double-differenced measurements, where, first, measurements from the same satellite, j are differenced between the two user receivers, denoted as A and B, to form single-differenced phase measurements

$$\Delta\phi^j_{A,B} = \lambda^{-1} r^j_{A,B} + \frac{c}{\lambda}\delta t_{A,B} + N^j_{A,B} + \varepsilon^j_{\phi,A,B} \qquad (2)$$

where the satellite clock bias errors are eliminated. Furthermore, when a short baseline between receivers A and B is assumed, as in our application with close formation flying UAVs, the troposphere and ionosphere delays are also considered as eliminated. In order to further eliminate the combined user receiver clock biases, $\delta t_{A,B}$, two single-differenced measurements from satellites j and k are subtracted to form double-differenced phase measurements, which are indicated as $\nabla\Delta\phi^{j,k}_{A,B}$. In practice, double-differences are often formed by selecting a high-elevation satellite as the reference satellite (indicated in this paper as k) and subtracting its single-difference measurement from all other available single-difference measurements (Blewitt, 1997). This ensures that the reference satellite will be likely be in view throughout the test duration and is not sensitive to local low-elevation masks. With double-differenced measurements, the only remaining errors are the multipath errors and the integer ambiguity.

To estimate the 3D relative position of the two UAVs, a nonlinear Unscented Kalman Filter (UKF) (Julier and Uhlmann, 1997) that is formulated to process measurements sequentially (Oh, 2010) is employed. For a description of the UKF algorithm, the reader is referred to (Simon, 2006), here ,we simply identify the state vector, x, measurement vector z, output vector, y, process model f, observation model h, as well as, the process noise Q and measurement noise R covariance assumptions used. These terms are related to each other in the filter's prediction step as

$$x_{k|k-1} = f(x_{k-1|k-1}) + w_k \tag{3}$$

and the measurement-update step as

$$y_{k|k-1} = h(x_{k|k-1}) + v_k \tag{4}$$

where the process-noise is assumed to be distributed $w_k \sim N(0,Q)$ and the measurement-noise is assumed to be distributed $v_k \sim N(0,R)$.

The state vector, x, consists of the 3D relative position vector between UAV_A and UAV_B and the phase ambiguities on the L1 and L2 double-differenced carrier phase measurements.

$$x = \begin{bmatrix} \Delta X & \Delta Y & \Delta Z & N_{L1}^{i\ldots n} & N_{L2}^{i\ldots n} \end{bmatrix} \tag{5}$$

The measurement vector, z, is made up of n double-differenced phase measurements for each the L1 and L2 frequencies, the dual-frequency ionospheric-free pseudo-range only, ρ_{IF}, least-squares estimated 3D relative position vector, $\begin{bmatrix} \Delta X & \Delta Y & \Delta Z \end{bmatrix}_{\rho_{IF}}$, and the IR-UWB peer-to-peer range between the UAVs, R_{UWB}.

$$z = \begin{bmatrix} \nabla\Delta\phi_{L1}{}_{A,B}^{i\ldots n,k} & \nabla\Delta\phi_{L2}{}_{A,B}^{i\ldots n,k} & \Delta X_{\rho_{IF}} & \Delta Y_{\rho_{IF}} & \Delta Z_{\rho_{IF}} & R_{UWB} \end{bmatrix} \tag{6}$$

The output-vector, y, has a one-to-one correspondence with the measurement vector, z, such that z represents the observed and y is the computed to form the filter's Observed-Minus-Computed (OMC) innovation residuals.

The observation function for an individual double-differenced phase measurement, h_ϕ, between satellite j and reference satellite,k, on frequency, f, (i.e. L1 or L2) is defined as

$$z_\phi = \nabla\Delta\phi_f{}_{A,B}^{j,k} = y_\phi = \begin{bmatrix} -(\underline{1}_A^j - \underline{1}_A^k)^T \end{bmatrix} \begin{bmatrix} \Delta X \\ \Delta Y \\ \Delta Z \end{bmatrix} + \lambda_f N_f^j + v_\phi \tag{7}$$

where the 3D relative position vector is from the filter prediction step, the phase ambiguity N_f^j is from the filter's prediction step, λ_f is the wavelength of the measurement (i.e. L1 or L2), $\underline{1}_A^j$ is the unit vector from receiver A to satellite j, and v_ϕ is the measurement noise assumed for double-differenced phase observables.

The observation function for the range-only 3D estimate relative position vector, $h_{\rho_{IF}}$, simply picks out the predicted 3D relative position vector and accounts for the measurement noise of the range-only position solutions

$$z_{3D_{\rho_{IF}}} = \begin{bmatrix} \Delta X \\ \Delta Y \\ \Delta Z \end{bmatrix}_{\rho_{IF}} = \begin{bmatrix} \Delta X \\ \Delta Y \\ \Delta Z \end{bmatrix} + v_{3D_{\rho_{IF}}} \tag{8}$$

where, again, the 3D relative position vector is from the filter prediction step.

The observation function of the UWB peer-to-peer range, h_{UWB} is the L_2 norm of the 3D relative position vector

$$z_{UWB} = R_{UWB} = y_{UWB} = \sqrt{\Delta X^2 + \Delta Y^2 + \Delta Z^2} + v_{UWB} \tag{9}$$

where the IR-UWB peer-to-peer measurement is used as direct measurement of the baseline separation between the GPS receiver antenna phase center on UAV_A and UAV_B and v_{UWB} is the noise assumed for the UWB measurement. Note that this formulation assumes that there no lever arm between the UWB radio antennas and the GPS antenna phase centers, but in practice, this must be accounted for, and will be addressed is future works.

The measurement-error covariance matrix assumes 1 meter-level errors in the range-only 3D relative navigation solution, $v_{\rho_{IF}}$ and 1 cm-level noise on the double-differenced phase measurements, v_ϕ, such that there 100-to-1 data weighting in favor differential phase measurements. Nominally, 10 cm measurement error is assumed for UWB measurement, v_{UWB}, however, this is later varied in the simulation study. Therefore, the measurement-error covariance, R, is of the form

$$R = diag(\begin{bmatrix} v_{\phi,1}^2 & \ldots & v_{\phi,n}^2 & v_{\rho_{IF}}^2 & v_{\rho_{IF}}^2 & v_{\rho_{IF}}^2 & v_{UWB}^2 \end{bmatrix}) \tag{10}$$

The 3D relative position vector states are modeled as random-walk and the phase bias states are assumed to be random constants, therefore, the prediction model for the 3D navigation vector, f_{3DRel}, is of the form

$$x_{k|k-1} = x_{k-1|k-1} + w_{3D} \tag{11}$$

and the prediction model of the phase biases, f_ϕ, is

$$x_{k|k-1} = x_{k-1|k-1} \tag{12}$$

where the process-noise is zero. This is the case as long the tracking of a particular satellite and the reference satellite is continuous on both receivers used for the DGPS solution.

A each time-step, 1-meter of process-noise, w_{3D} is added to the 3D relative navigation states, such that the process-noise covariance matrix is $Q = diag(\begin{bmatrix} w_{3D}^2 & w_{3D}^2 & w_{3D}^2 \end{bmatrix})$.

In the event that a phase break occurs for a particular satellite on either GPS receiver, a white-noise reset is performed on its respective double-differenced phase ambiguity state. For the purposes of this paper, the occurrence

of a phase break is assumed to be known *a priori* through the use of a dual frequency data editing algorithm, such at the popular approach offered by Blewitt (Blewitt, 1990). In particular, a white-noise reset consists of setting the estimated phase bias to zero, setting the estimated variance of the phase bias to a large value (e.g. one second at the speed of light, and zero-ing out the covariances of the phase ambiguity state and the other filter parameters.

After each measurement update, the UKF estimated phase ambiguities, which do not take advantage of the fact that they are an integer number of wavelengths, are fed into the LAMBDA algorithm along with their UKF estimated variance-covariance matrix in order to determine integer-fixed ambiguity estimates. The freely available TU-Delft LAMBDA Toolbox (Joosten, 2001) was used for this implementation and the specific method employed used the ratio-test as an acceptance test for the integer-fixed biases. With the integer-fixed biases, the 3D relative navigation states are updated accordingly, by assuming that the integer fixing is a deterministic process, using the following equation

$$x_{3D,fix} = x_{3D,float} - P_{3DxPB}P_{PBxPB}(x_{PB,float} - x_{PB,fix}) \quad (13)$$

where P refers to the UKF estimated variance-covariance matrix, which particular sections identified by the subscripts $3D$,which refers to the relative position vector states and PB, which refers to phase ambiguity states. Bias fixing is done in a complimentary manner to the UKF, such that the fixed ambiguities and the associated adjusted 3D relative navigation states are not fed to the next filter step, but are instead saved as a separate estimate.

2.2 Tightly-Coupled Single-Difference Dual-Epoch GPS and Ultra-Wideband Ranging

The second formulation considers the use of a single-differenced dual epoch (SDSE) differential combination. This differential combination was developed and investigated within (Hedgecock et al., 2013) as a means to take advantage of the precise phase measurements and avoid the need for GPS phase integer ambiguity resolution. SDSE retains single-differences to retain geometric diversity that is lost when time differencing double-differences (i.e. triple differencing)(Misra and Enge, 2006), and uses a backward-difference time derivate to eliminate the unknown integer ambiguity by taking advantage of the fact that is remains unchanged as long as a link is continuously tracked. However, with single-differenced measurements, the combined user receiver clock bias $\delta t_{A,B}$ from Eq. 2 remains an error source that must be estimated. In particular, when using SDSE data, the time-derivative of this error-source, $\delta\delta t_{A,B}$ must be estimated. Using SDSE differential phase data is explored in this study in conjunction with the IR-UWB range measurements to determine if similar accuracy to bias-fixing can be obtained while avoiding the need for integer ambiguity resolution.

The state vector, x, of this formulation is the 3D relative position vector between the UAVs and its change over a single-epoch.

$$x = \begin{bmatrix} \Delta X & \Delta Y & \Delta Z & \delta\Delta X & \delta\Delta Y & \delta\Delta Z & \delta\delta t_{A,B} \end{bmatrix} \quad (14)$$

The measurement vector, z, consists of the SDSE phase data on L1 and L2, the psuedo-range-only estimated 3D position vector, and the UWB range measurement, R_{UWB}.

$$z = \begin{bmatrix} \left(\Delta\phi_{L1}{}_{A,B}^{i\ldots n}(t) - \Delta\phi_{L1}{}_{A,B}^{i\ldots n}(t-\Delta t)\right) \\ \left(\Delta\phi_{L2}{}_{A,B}^{i\ldots n}(t) - \Delta\phi_{L2}{}_{A,B}^{i\ldots n}(t-\Delta t)\right) \\ \Delta X_{\rho_{IF}} \\ \Delta Y_{\rho_{IF}} \\ \Delta Z_{\rho_{IF}} \\ R_{UWB} \end{bmatrix}^T \quad (15)$$

where Δt is the sampling period of the GPS data.

The observation function for the SDSE phase measurements, h_{SDSE} for satellite, j ,on frequency, f is given as

$$z_{SDSE} = \Delta\phi_{f}{}_{A,B}^{j}(t) - \Delta\phi_{f}{}_{A,B}^{j}(t-\Delta t) =$$

$$y_{SDSE} = (\underset{\sim}{1}_A^j)^T \begin{bmatrix} \delta\Delta X \\ \delta\Delta Y \\ \delta\Delta Z \end{bmatrix} + \delta\delta t_{A,B} + v_{SDSE}$$

where the estimates of change, δ, in the 3D relative position vector and combined receiver clock bias of UAV_A and UAV_B are from the prediction step and v_{SDSE} is the measurement noise assumed for the SDSE phase measurements.

The observation functions for the range-only 3D measurement vector elements, $h_{3D_{\rho IF}}$ and UWB range, h_{UWB}, are the same is in the first sensor fusion formulation in Eq. 8 and Eq. 9, respectively.

The measurement-error covariance matrix assumes 2-cm noise on the SDSE phase measurements, v_{SDSE}, such that there is a 50-to-1 data weighting in favor differential phase measurements. The assumed measurement noise for UWB, v_{UWB} and the range-only 3D position vector, $v_{\rho_{IF}}$, are the same as the previous formulation, such that the measurement-error covariance, R is give as:

$$R = diag(\begin{bmatrix} v_{SDSE,1}^2 & \cdots & v_{SDSE,n}^2 & v_{\rho_{IF}}^2 & v_{\rho_{IF}}^2 & v_{\rho_{IF}}^2 & v_{UWB}^2 \end{bmatrix} \quad (16)$$

In this formulation, the 3D relative position vector states are predicted using a single step integration of the previous estimated change in the 3D position vector plus process noise, f_{3D},

$$\begin{bmatrix} \Delta X \\ \Delta Y \\ \Delta Z \end{bmatrix}_{k|k-1} = \begin{bmatrix} \Delta X \\ \Delta Y \\ \Delta Z \end{bmatrix}_{k-1|k-1} + \begin{bmatrix} \delta\Delta X \\ \delta\Delta Y \\ \delta\Delta Z \end{bmatrix}_{k-1|k-1} + w_{3D} \quad (17)$$

where w_{3D} is 1-meter of process noise as in the previous formulation. The remaining states, including the single

time-step change in the 3D position vector and combined clock bias of receiver A and receiver B are modeled as white-noise, such that their prediction model is a simple white-noise update.

$$x_{k|k-1} = w \tag{18}$$

The process-noise assumed for the change is the 3D position vector in a single time step, $w_{\delta 3D}$, is 10 meters and the change in the receivers combined clock bias, $w_{\delta\delta t_{A,B}}$ is 30-meters (i.e. 0.1 micro-second), such that the assumed process-noise covariance is

$$Q = diag(\begin{bmatrix} w_{3D}^2 & w_{3D}^2 & w_{3D}^2 & w_{\delta 3D}^2 & w_{\delta 3D}^2 & w_{\delta 3D}^2 & w_{\delta\delta t_{A,B}}^2 \end{bmatrix}) \tag{19}$$

.

In this formulation, whenever a phase break occurs, the assumption that the backward difference time-derivate will eliminate the phase ambiguity in the SDSE phase measurement is invalid. As such, a phase break results in a gross data outlier that is easily detectable by evaluating the post-fit residuals epoch-wise. Therefore, in this formulation a detection threshold on the post-fit residuals (chose as 20 meters) was used to identify and delete data outliers. In this study, breaks are assumed known, and therefore outlier measurements SDSE phase measurements were flagged *a priori* and not included in the filter solution.

3 WVU *PHASTBALL* RESEARCH UAV

The WVU *Phastball* aircraft was designed to be a modular and low-cost UAV platform that can support a wide range of flight research topics. In uses a custom designed flexible avionics package (Gu et al., 2012) which will be upgraded to include a ranging radio in order to experimentally validate the results of this simulation study. The *Phastball* design, shown in Figure 1 , has a 2.4 meter wingspan and a 2.2 meter total length. The typical takeoff weight is 10.5

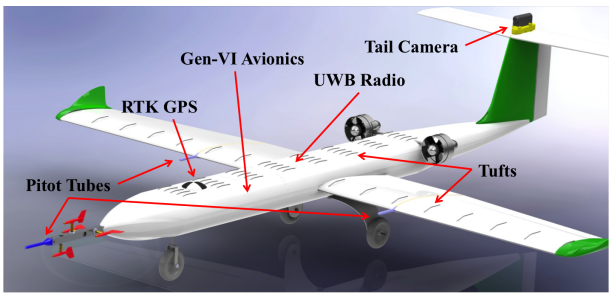

Figure 1. WVU *Phastball* Research UAV design with main components indicated.

Kg with a 3.2 Kg payload capacity. The aircraft is propelled by two brushless electric ducted fans, each providing up to 30 N of static thrust, offering a cruise speed of approximately 30 m/s. The *Phastball* has been proven to be a low-cost, low-maintenance, easy to operate, multi-functional, and highly effective research tool with over 240 flight test experiments were performed using four *Phastball* aircraft in recent years, including recent close formation flight experiments, as shown in Figure 2.

Figure 2. Summer 2013 *Phastball* close-formation flight.

4 SIMULATION ENVIRONMENT

The simulation environment developed for this study incorporates WVU's *Phastball* Formation Flight simulation environment (WVU-FF-Sim) with GPSoft's SatNav 3.04 Matlab Toolbox (GPSoft, 2003). In particular, the WVU-FF-Sim is used to generate UAV leader and follower trajectories, of which GPS observables with realistic error sources are generated by the SatNav 3.04 Toolbox.

The WVU-FF-Sim incorporates dynamic models for the WVU *Phastball* UAV of which the parameters were derived using recording flight data (McGrail, 2012). Furthermore, it incorporates Nonlinear Dynamic Inversion (NLDI) formation flight control laws(Gu et al., 2006), of which WVU-FF-Sim's simulated formation control performance has been validated against actual formation flight tests (Larrabee, 2013). A bird's eye view of the trajectory simulation is shown in the top panel of Figure 3 where the typical baseline separation between the UAVs in this simulation is approximately 30 meters.

The SatNav-3.04 Toolbox incorporates several models to simulate GPS error sources and a few additional models were developed and incorporated for the purposes of this study. By default, thermal noise, ionospheric and tropospheric delays, multipath, and phase ambiguities are modeled and applied to simulated GPS observables. The thermal noise was modeled as 0.32 meters σ for the ranging error on psuedo-range measurements and 0.016λ meters σ for the carrier phase data. The multipath error was modeled as a Gauss-Markov process with a σ of 1.6 meters and a time constant of 2 minutes at full intensity (GPSoft, 2003). The tropospheric error model used in the ToolBox is based on the modified Hopfield algorithm (Goad and Goodman, 1974), and the ionospheric delay model is a raised half-cosine from (Parkinson and Spilker, 1996) that is scaled

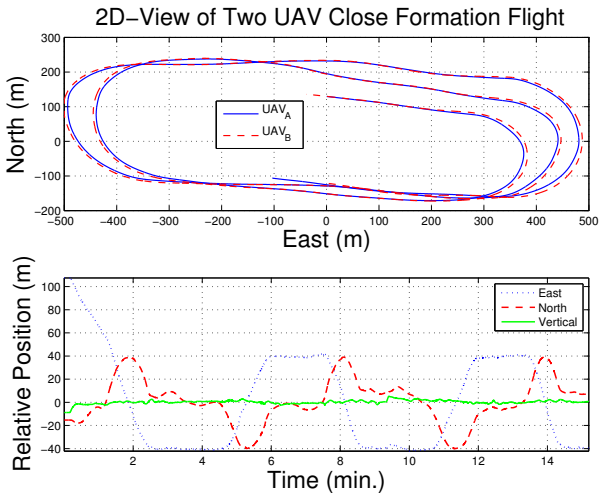

Figure 3. UAV Formation (top), ENU Formation Separation (bottom)

based on the FAA's WAAS obliquity factor from (Kaplan and Hegarty, 2005). Furthermore, a random initial bias and drift rate was assumed for each UAV's GPS receiver clock bias. The phase observables generated by the SatNav-3.04 ToolBox adds a constant ambiguity for each SVN, however, this was modified to be a randomly initialized value that could optionally shifter at any epoch. This allowed the ability to simulate phase breaks, and using this feature, phase breaks were simulated to occur more often during periods in which the UAV is experiencing a large bank angles. With this approach, a user selectable break likelihood was chosen along with a roll angle threshold, for example, Figure 4 shows the $\nabla\Delta\phi_{L1}$ arcs when of a 2% likelihood of a phase break occurring for roll angles greater than 30°.

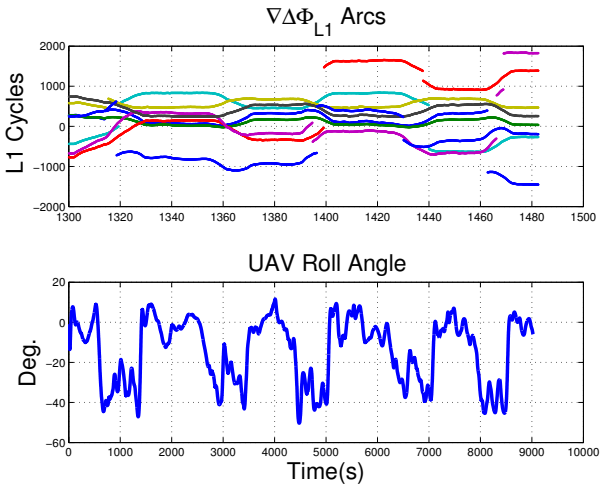

Figure 4. $\nabla\Delta\phi_{L1}$ arcs where the discontinuities indicate simulated phase breaks (top), Corresponding roll angle of UAV_A

In Figure 4 if there were no phase breaks the individual $\nabla\Delta\phi_{L1}$ arcs would be continuous.

5 UWB INTEGRATION TRADES

The UWB ranging radios considered in this work enable precise distance measurement while providing wireless data transfer between vehicles are PulsON 410 models commercially available from Time Domain. The use of these radios, pictured in Figure 5 (Time-Domain, 2014) present a trade-off between measurement rate, maximum link distance, and data throughput is described in this section.

Figure 5. Time Domain P410 Ranging Radio [reproduced with permission from (Time-Domain, 2014)]

5.1 Signaling Model

The UWB radios implement a pulsed rather than sinusoidal basis in order to enhance distance measurement accuracy, especially in the presence of multi-path. This pulse basis is constructed into an iterative stream with pseudo-random delay between pulses to support spectral power limits while providing multi-link channelization. The signal model, simplified from (Win and Scholtz, 1998):

$$s_{tr}^{(k)} = A_k \sum_{j=-\infty}^{\infty} d_{\left[\frac{j}{N_s}\right]}^{(k)} w_{tr}(t^{(k)} - jT_f - c_j T_c) \qquad (20)$$

where A_k is an amplitude normalization factor of transmitter k, a preconfigured value limited by FCC regulations for unlicensed operation (FCC, 2002), w_{tr} is a single pulse waveform (depicted in Figure 6), $t^{(k)}$ is the k_{th} transmitter's clock time, T_f is the mean pulse repetition interval (PRI), c_j is a pseudo-random time hopping sequence, common to transmitter and receiver(s) on the same channel, T_c is the duration of delay based on the repeating pattern at index c, and $d_{\left[\frac{j}{N_s}\right]}^{(k)}$ is a binary modulation sequence from the binary set [-1,1] implementing bi-phase shift keying or "flip" modulation with symbol dwell duration N_s.

P410 user-configurable parameters include A_k, (i.e. "tx_{gain}") which has direct impact on the transmit power

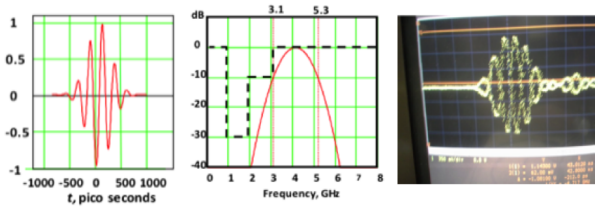

Figure 6. Time and frequency representation of the pulse model along with an actual oscilloscope measurement demonstrating the Bi-phase Signal Keyed (BPSK) or "flip" modulation.

P_t, the parameters T_f, c_j, and T_c are included in the user-selectable code channel, and $N_s = 2^P II$ where PII is the user-configurable "Pulse Integration Index". The user-adjustable PII improves signal to noise through coherent pulse integration; configuration of this parameter on both requesting and responding radios dictates the maximum link distance.

5.2 Link Budget Model

The maximum link distance at various PII values is modeled by a simplified Friis equation as follows:

$$SNR = \frac{P_t G_{ant} N_s}{D_{max} r^{\alpha} L_{sys}} \tag{21}$$

where SNR is the signal to noise ratio at the receiver front end, P_t is the transmit power (-13.5dBm), G_{ant} is the combined gains of both the transmitter and receiver antennas (normalized to 0dB using default Broadspec^{TM} antennas), $N_s = 2^{PII}$ is the number of pulses integrated in each symbol, D_{max} is the pulse repetition rate (10MHz), and r is the distance between transmitter and receiver, raised to the pathloss exponent α. α is assumed 2 in this line-of-sight (LOS) application. L_{sys} is a catch-all system loss and normalization factor determined through a 1 meter line-of-sight link measurement which was determined through experimentation to be 116dB.

Based on this model, further experimentation through variable attenuation indicates approximately 12dB SNR is required to achieve 95% acquisition performance. Given this link budget model with constant transmit power and antenna gain the maximum ranging distance, D_{max}, versus versus PII can be derived as expressed in Figure 7 (top of next page).

5.3 Packet Structure and Range Conversation

As described previously, the number of pulses per symbol $N_s = 2^{PII}$ dictates the maximum link distance. However, increasing PII also lengthens the packet duration, and therefore decreases the measurement rate and data rate. Adding user data also extends packet duration therefore decreasing measurement rate.

Figure 8 describes the packet structure as four distinct frames: acquisition preamble, link header (containing packet type as well as unique source and sink node identifiers, ranging frame (enabling signal scanning required to isolate the first, most direct-path energy), ending with an optional user data frame of variable length.

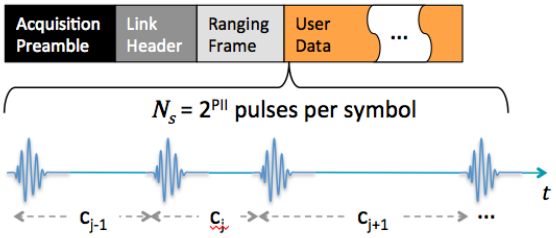

Figure 8. Pulses are structured into packet frame components.

Packets used for precision distance measurement are paired into "ranging conversations", each consisting of a "request packet" followed by a "response packet". As depicted in Figure 9 a complete ranging conversation begins, after optional reconfiguration, with the requesting host initiating a ranging conversation which causes its co-located radio to send a targeted request packet while triggering a high-precision clock. Upon reception of the request packet the targeted responder, after a precise, well-known delay, transmits a response packet. Once the requesting radio has receiving the response it computes the Two-Way Time-of-Flight (TW TOF) distance from the delay, corrected by direct path offset estimate, then passes this distance to the initiating host. Note that both the request packet and response packet may contain user data, which is also available to any other promiscuously receiving radios in the neighborhood.

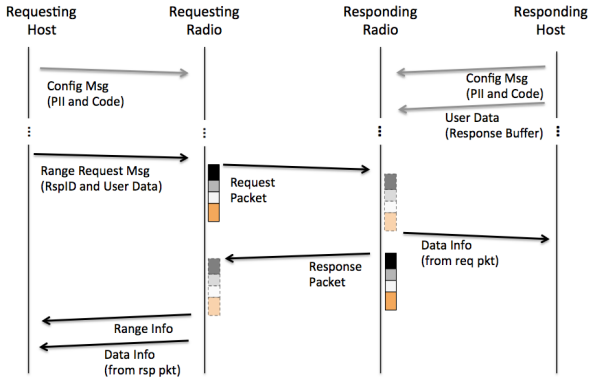

Figure 9. A notional time progression of a host-initiated Two-Way Time-of-Flight (TOF) distance measurement.

5.4 Relating D_max, Data Throughput, and Measurement Rate

Based on the foundation models described previously, it becomes apparent that optimal configuration of a ranging radios requires trade-off between maximum distance, data

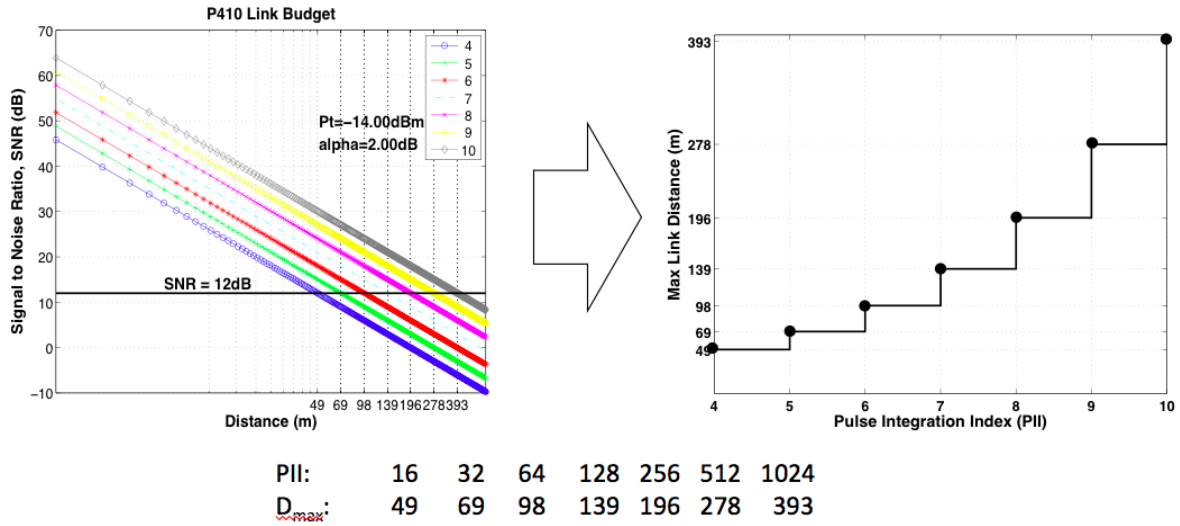

Figure 7. Determination of maximum link distance, D_{max}, versus available pulse integration index values ($PII = log2(N_s)$).

throughput, and update rate required for operation. Figure 10 provides a graphical description of this trade space. For the subject leader-follower UAV application one may assume an operational separation less than 200m. Thus a PII=8, allowing 196m, may suffice. Further assuming a measurement rate of 10Hz is sufficient, the graph indicates that up to 256 bytes can be transmitted per conversation. At a conversation/measurement rate of 10Hz this results in a total throughput of 2.56KBytes/s available, which can be shared between requesting and responding radios.

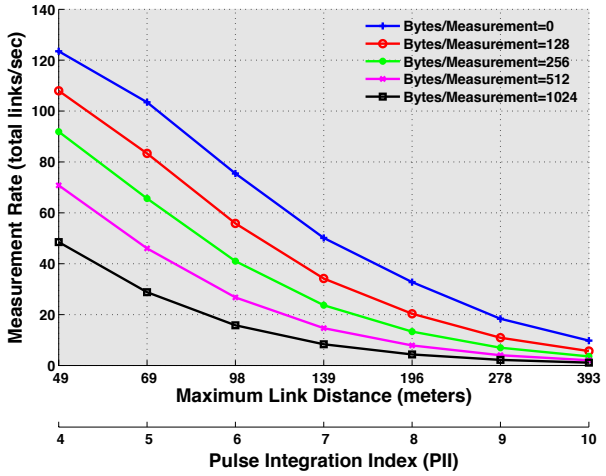

Figure 10. The relationship between Range Conversation Duration versus a combination of *PII* and Data words

6 RESULTS AND DISCUSSION

To gain insight into the potential benefits of including IR-UWB peer-to-peer ranging for augmenting DGPS relative navigation, the sensitivity of estimation performance under various conditions are analyzed using a set of multiple simulation trials. The error metric utilized is 3D Residual Sum of Square that combines the RMS error on each the X, Y, and Z relative navigation axes.

$$E_{3D_{RSS}} = \sqrt{E^2_{X_{RMS}} + E^2_{Y_{RMS}} + E^2_{Z_{RMS}}} \tag{22}$$

where the RMS is calculated of the estimated filter state against the simulation truth.

First, estimation error performance sensitivity of the presented formulations is monitored against increasing multipath intensity. For this analysis, 5 simulation trials were executed each with new randomly generated error sources were included on the GPS and UWB measurements, while increasing the multipath error intensity from low-multipath to full intensity (i.e. full $\sigma = 1.6m$, $\tau = 2$ min). For every simulation in this analysis, phase breaks were included with a likelihood of occurrence of 0.5% for roll angles above 30°, and σ_{UWB} was modeled as 10 cm. Figure 11 shows the mean of the 50 trials for 10 multipath intensities. In Figure 11 the estimation error for the LAMBDA integer fixed and floating phase ambiguities with and without including UWB measurements is shown, as well as the SDSE algorithm with and without UWB ranging. Overall, the SDSE algorithm is not as good as processing the double-difference phase arcs. The benefit of the UWB ranging is clear as multipath increases. Under low multipath conditions, the bias fixed estimation error with and without UWB is nearly identical and under 10-cm. As the multipath intensity increases, the fixed solution with no UWB measurements degrades more rapidly than is UWB counterpart, suggesting that integer biases may be fixed incorrectly. That is, within Figure **??**, while many individual trials were able may have had the majority of flights that had all epochs successfully fixed, some starts started to fail to correctly fix, increasing the mean of the 50 trials. The

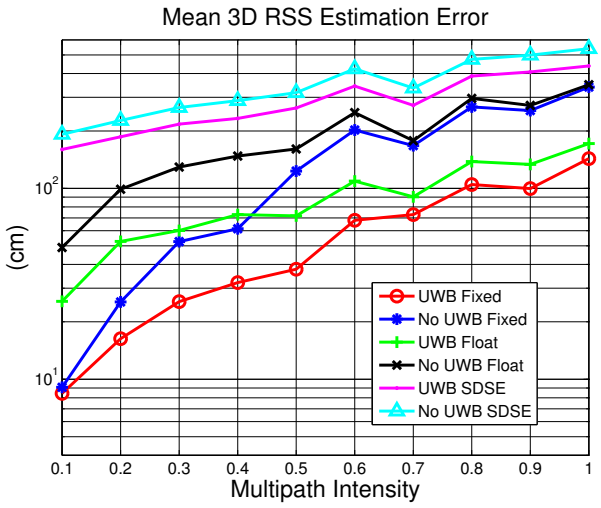

Figure 11. 3D RSS relative navigation error vs. multipath error intensity. LAMBDA fixed and float bias solution with and without UWB ranging.

UWB solution, even without bias fixing (i.e. green series with + marks), is more robust than the LAMBDA bias fixed without UWB ranging . The total $3D_{RSS}$ stays decimeter-level meter on average over the 50 trials for the fixed UWB solution all the but highest multipath environment. Not that when interpreting

The next set of 50 trials held the multipath intensity at 0.3 and σ_{UWB} to 10 cm and increased the frequency of phase breaks. That is, the likelihood of the occurrence of a phase break when the UAVs are above 30°roll was varied from 0.5% to 5%.

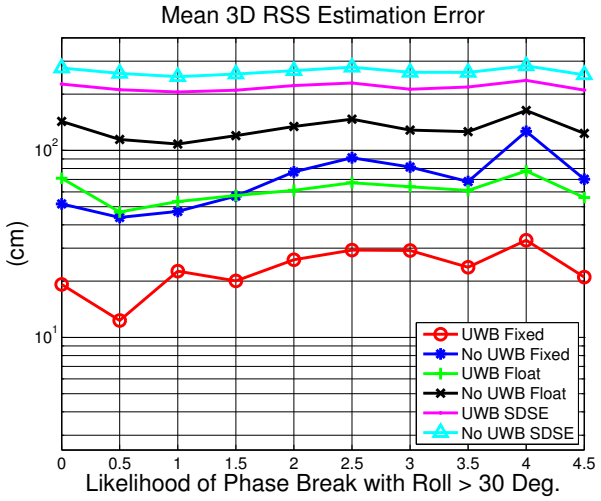

Figure 12. 3D RSS relative navigation error vs. likelihood of phase break when roll angles exceed 30 degrees. LAMBDA fixed and float bias solution with and without UWB ranging.

In Figure 12 the estimation error remains relatively flat at $\sim$ less than 20-cm as the likelihood of (i.e. number of) phase breaks increases for the UWB fixed and float solutions. This indicates that that UWB measurements are effective at allowing the float estimated phase ambiguities to converge close enough to their actual integer values that the LAMBA algorithm is effective within a short period of time. Again, the float UWB solution is competitive with the non-UWB aided bias fixed solution and the SDSE algorithm is not as good.

The next set of simulation trials deals with the practical multi-sensor integration issue of time alignment. In particular, the estimation performance sensitivity against increasing measurement lag of the IR-UWB measurement with respect to the GPS measurements is evaluated. During these simulation trials, the multipath intensity was held at 0.3 , the break likelihood above 30°roll was held at 0.5%, and the σ_{UWB} was held at 10-cm. The mean of the 50 trials for each UWB measurement lag condition ranging form 0 to 0.5 seconds is shown in Figure 13. For this simulation, only Formulation 1 with and without ambiguity resolution was considered, as it clearly outperforms that SDSE approach.

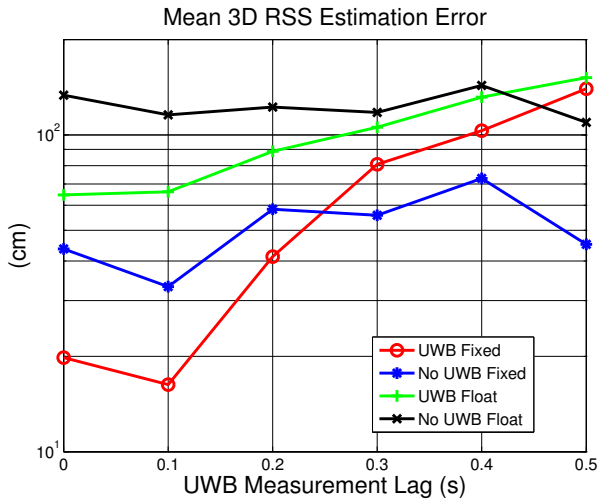

Figure 13. 3D RSS relative navigation error vs. time lag of UWB measurements with respect to GPS measurements. LAMBDA fixed and float bias solution with and without UWB ranging.

The trend of Figure 13 suggests that for the this particular UAV formation flight application, or applications with similar relative navigation dynamics, the UWB measurement is still beneficial even if it is lagged by up to $\sim$0.25 seconds with respect to the GPS measurements. This is encouraging as this level of time alignment is easily achievable even without any sophisticated timing hardware implementation, and is presented only as a practical implementation consideration for implementation in low-cost systems.

Finally, the benefit of the UWB ranging source is evaluated with respect to its measurement error. That is,

σ_{UWB} is varied from 2.5 cm to 50 cm. Under best performance, 2.5 cm is reported as achievable for IR-UWB ranging (Time-Domain, 2014) , however it is worth considering that this may actually not be the case for a particular set-up. For these simulation trials, it is assumed that the UWB estimation error is well characterized, such that the Kalman estimator uses a proper σ_{UWB} in its measurement-error covariance matrix, R, assumption. Figure 14 shows the mean of 50 simulation trials at each various σ_{UWB}, with the multipath intensity held a 0.3 and phase break likelihood held at 0.5% beyond 30 degrees roll. Again, for these simulation trials, only Formulation 1 with and without ambiguity resolution was considered, as Formulation 1 clearly outperforms that SDSE approach.

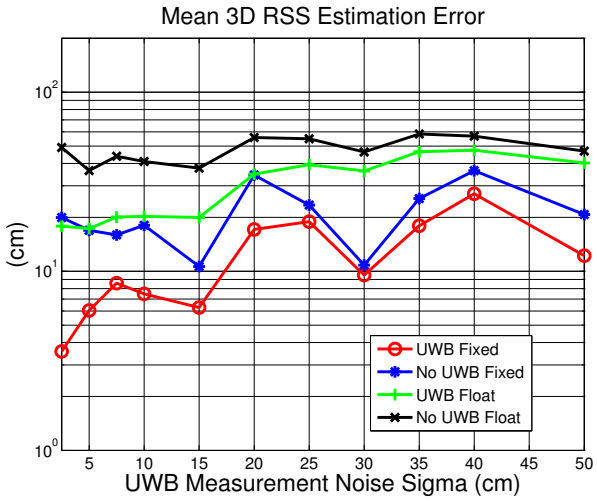

Figure 14. 3D RSS relative navigation error vs. σ_{UWB}. LAMBDA fixed and float bias solution with and without UWB ranging.

Figure 14 shows the encouraging result that the UWB measurements do not have to be incredibly accurate to provide a benefit in 3D relative estimation performance. As expected, the separation between the $3D_{RSS}$ of the estimation error of the fixed UWB solution and fixed non-UWB solution is greater with very accurate UWB measurements (UWB is more beneficial). However, even at 0.5 meter σ_{UWB} the UWB solutions still outperformed their non-UWB counterparts.

7 CONCLUSIONS AND FUTURE WORK

In light of the fact that IR-UWB devices are a low Size Weight and Power device readily available for incorporation, this paper considered the incorporation of IR-UWB peer-to-peer range measurements to assist DGPS relative navigation algorithms in the context of UAVs flying in close formation. Two different formulations were presented and a simulation environment was used to offer a characterization of the potential benefit of incorporating IR-UWB peer-to-peer ranges when confronted with scenarios that are known to typically degrade DGPS performance including: heightened multipath and lots of phase breaks. Furthermore, a trade analysis for UWB integration in terms of max range distance, communication throughout and update rate for the Time Domain P-410 module was presented. Similarly, the sensitivity to the time-lag of the IR-UWB ranges with respect to GPS measurements and UWB measurement noise were also considered.

Under the various scenarios considered, the benefit of incorporating this type of ranging sensor is quite clear. Under nearly ideal conditions, the DGPS solution with and without IR-UWB ranges included exhibit very similar estimation performance. However, as error sources are increased, the solutions with an IR-UWB maintain better overall performance on average.

It is important to discuss the limitations of this simulation study. For example, the effects on estimation performance due to different satellite geometries is not captured within these results. That is, a single flight test was repeated under different error source conditions, but the same geometry was simulated. Varying satellite geometry may offer additional important insights. Second, the expected added robustness of RTK DGPS's ability to recover with the addition of Inertial Navigation Systems is not considered. Finally, it is noted that a simulation such this is not a substitute for the value of collecting and processing real flight data.

The next immediate step of this work to the verify these results using real flight data collected on the WVU *Phastball* UAV. Further developments will include the incorporation of Inertial Measurement Unit (IMU) data on each of the UAVs as well as accounting for each sensors lever arm with respect to the UAV center of gravity. Ultimately a real-time implementation will be evaluated as the primary relative navigation feedback within close formation flight control. The potential for DGPS/UWB fusion is not only the increased robustness for relative navigation performance, as considered here, but perhaps more importantly, the potential for cooperative navigation implementations in which multiple vehicles share GPS observation to increase their overall solution robustness.

ACKNOWLEDGEMENTS

J. Gross was supported for this work by the NASA WV EPSCoR and WV Research Challenge Fund seed grant Program. Y. Gu was supported by NASA Grant #NNX14AF55A.

REFERENCES

G. Blewitt. An automatic editing algorithm for gps data. *Geophysical Research Letters*, 17(3):199–202, 1990.

G. Blewitt. Basics of the gps technique: observation equations. *Geodetic applications of GPS*, pages 10–54, 1997.

E. Broshears. *Ultra-wideband Radio Aided Carrier Phase*

Ambiguity Resolution in Real-Time Kinematic GPS Relative Positioning. PhD thesis, Auburn University, 2013.

F. C. C. FCC. Fcc 02-48 first report and order. `http://transition.fcc.gov/Bureaus/Engineering_Technology/Orders/2002/fcc02048.pdf`, 2002.

C. Goad and L. Goodman. Modified hopfield tropospheric refraction correction model. In *TRANSACTIONS-AMERICAN GEOPHYSICAL UNION*, volume 55, pages 1106–1106. AMER GEOPHYSICAL UNION 2000 FLORIDA AVE NW, WASHINGTON, DC 20009, 1974.

GPSoft. Satellite navigation toolbox 3.0 user's guide. 2003.

Y. Gu, B. Seanor, G. Campa, M. R. Napolitano, L. Rowe, S. Gururajan, and S. Wan. Design and flight testing evaluation of formation control laws. *Control Systems Technology, IEEE Transactions on*, 14(6):1105–1112, 2006.

Y. Gu, J. Gross, F. Barchesky, H. Chao, and M. Napolitano. Avionic design for a sub-scale fault tolerant flight control test-bed. *Chapter*, 21:499–522, 2012.

W. Hedgecock, M. Maroti, J. Sallai, P. Volgyesi, and A. Ledeczi. High-accuracy differential tracking of low-cost gps receivers. In *Proceeding of the 11th annual international conference on Mobile systems, applications, and services*, pages 221–234. ACM, 2013.

Y. Jiang. Integration of uwb ranging and gps for improved relative vehicle positioning and ambiguity resolution. 2012.

P. Joosten. The lambda-method: Matlabtm implementation. 2001.

S. J. Julier and J. K. Uhlmann. A new extension of the kalman filter to nonlinear systems. In *Int. symp. aerospace/defense sensing, simul. and controls*, volume 3, pages 3–2. Orlando, FL, 1997.

E. D. Kaplan and C. J. Hegarty. *Understanding GPS: principles and applications*. Artech house, 2005.

T. J. Larrabee. Wind and wake sensing with uav formation flight: System development and flight testing. 2013.

G. MacGougan, K. O'Keefe, and R. Klukas. Tightly-coupled gps/uwb integration. *Journal of Navigation*, 63 (01):1–22, 2010.

A. K. McGrail. *OnBoard Parameter Identification for a Small UAV*. West Virginia University, 2012.

P. Misra and P. Enge. *Global Positioning System: Signals, Measurements and Performance Second Edition*. Lincoln, MA: Ganga-Jamuna Press, 2006.

S.-M. Oh. Multisensor fusion for autonomous uav navigation based on the unscented kalman filter with sequential measurement updates. In *Multisensor Fusion and Integration for Intelligent Systems (MFI), 2010 IEEE Conference on*, pages 217–222. IEEE, 2010.

B. W. Parkinson and J. J. Spilker. *Progress In Astronautics and Aeronautics: Global Positioning System: Theory and Applications*, volume 2. Aiaa, 1996.

D. Simon. *Optimal state estimation: Kalman, H infinity, and nonlinear approaches*. John Wiley & Sons, 2006.

P. J. Teunissen. The least-squares ambiguity decorrelation adjustment: a method for fast gps integer ambiguity estimation. *Journal of Geodesy*, 70(1-2):65–82, 1995.

Time-Domain. P-410 ultra wideband ranging and communications module. `http://www.timedomain.com/datasheets/TD_DS_P410_RCM_FA.pdf`, 2014. Accessed: 2014-07-12.

W. Williamson, T. Rios, and J. L. Speyer. Carrier phase differential gps/ins positioning for formation flight. In *American Control Conference, 1999. Proceedings of the 1999*, volume 5, pages 3665–3670. IEEE, 1999.

W. R. Williamson, M. F. Abdel-Hafez, I. Rhee, E.-J. Song, J. D. Wolfe, D. F. Chichka, and J. L. Speyer. An instrumentation system applied to formation flight. *Control Systems Technology, IEEE Transactions on*, 15(1): 75–85, 2007.

M. Z. Win and R. A. Scholtz. Impulse radio: How it works. *IEEE Communications letters*, 2(2):36–38, 1998.